

# P-bodies directly regulate MARF1-mediated mRNA decay in human cells

William R. Brothers<sup>1</sup>, Hana Fakim<sup>1</sup>, Sam Kajjo<sup>1</sup> and Marc R. Fabian<sup>1,2,3,\*</sup>

<sup>1</sup>Lady David Institute for Medical Research, Jewish General Hospital, Montreal, Quebec, H3T 1E2, Canada, <sup>2</sup>Department of Biochemistry, McGill University Montreal, Quebec, H3A 1A3, Canada and <sup>3</sup>Gerald Bronfman Department of Oncology, McGill University Montreal, Quebec, H3A 1G5, Canada

Received February 16, 2022; Revised June 10, 2022; Editorial Decision June 13, 2022; Accepted June 15, 2022

## ABSTRACT

**Processing bodies (P-bodies) are ribonucleoprotein granules that contain mRNAs, RNA-binding proteins and effectors of mRNA turnover. While P-bodies have been reported to contain translationally repressed mRNAs, a causative role for P-bodies in regulating mRNA decay has yet to be established. Enhancer of decapping protein 4 (EDC4) is a core P-body component that interacts with multiple mRNA decay factors, including the mRNA decapping (DCP2) and decay (XRN1) enzymes. EDC4 also associates with the RNA endonuclease MARF1, an interaction that antagonizes the decay of MARF1-targeted mRNAs. How EDC4 interacts with MARF1 and how it represses MARF1 activity is unclear. In this study, we show that human MARF1 and XRN1 interact with EDC4 using analogous conserved short linear motifs in a mutually exclusive manner. While the EDC4–MARF1 interaction is required for EDC4 to inhibit MARF1 activity, our data indicate that the interaction with EDC4 alone is not sufficient. Importantly, we show that P-body architecture plays a critical role in antagonizing MARF1-mediated mRNA decay. Taken together, our study suggests that P-bodies can directly regulate mRNA turnover by sequestering an mRNA decay enzyme and preventing it from interfacing with and degrading targeted mRNAs.**

## INTRODUCTION

The decay of mRNA populations is a tightly regulated process that is essential for cells to properly execute gene expression programs. In general, mRNA turnover is initiated through trimming of the poly(A) tail by the CCR4–NOT complex (1), followed by the recruitment of the mRNA decapping complex to the 5' end of the mRNA. The mRNA decapping complex is comprised of the DCP2 decapping enzyme along with its decapping co-factor DCP1A, and en-

hancer of decapping proteins (EDC proteins; i.e. EDC3 and EDC4) (2). The mRNA decapping complex mediates the hydrolysis of the 5' N<sup>7</sup>-methylguanosine cap structure from the mRNA, which generates a monophosphate at the 5' end that commits the mRNA for degradation by the XRN1 exonuclease. Human XRN1 associates with the mRNA decapping complex through a direct interaction with EDC4, which has been reported to accelerate the efficient decay of nascently decapped mRNAs (2,3). The process of 5'-3' mRNA decay is often initiated by RNA binding proteins that bind mRNA 3'UTRs and act as platforms that recruit the CCR4–NOT complex to targeted mRNAs (4,5).

In addition to their roles in regulating mRNA decay, RNA-binding proteins and their cognate mRNAs can phase-separate into ribonucleoprotein (RNP) granules that assemble through multivalent RNA–RNA, RNA–protein and protein–protein interactions (6). These interactions drive the formation of microscopically visible foci through liquid–liquid phase separation and can be defined by characterizing their components. A well-known class of cytoplasmic RNP granules are processing bodies (P-bodies), which are comprised of mRNAs complexed with proteins that play roles in translational repression, deadenylation, mRNA decapping, and 5'-3' decay. These include core proteins such as EDC4, LSM14A, 4E-T, and DDX6 (7–10). P-bodies were initially thought to be sites of mRNA decay, given their concentration of decay factors and that blocking mRNA decay pathways can lead to their dissolution (11). However, more recent work has postulated that rather than being sites of mRNA decay, P-bodies contain stable mRNAs that are translationally repressed (12–14). Notwithstanding these advances in characterizing P-body components and the mRNAs enriched within them, attempts to establish causal roles for P-bodies in regulating mRNA translation and/or decay has remained elusive.

Another RNA-binding protein that associates with P-bodies is the mammalian endoribonuclease MARF1 (meiosis regulator and mRNA stability factor 1) (15–17). MARF1 plays an essential role in promoting mammalian oogenesis; female MARF1 knock-in mice that harbor inactivating mutations within the NYN endonuclease domain

\*To whom correspondence should be addressed. Tel: +1 514 340 8222 (Ext 28575); Email: marc.fabian@mcgill.ca

generate fertilization-incompetent oocytes that arrest at the germinal vesicle stage, failing to undergo proper meiotic maturation (18,19). MARF1 is also somatically expressed and has been reported to play a role in promoting cortical neurogenesis (20). In general, MARF1 binds the 3'UTRs of targeted mRNAs using a core of tandem RNA-binding LOTUS domains and mediates their decay using its NYN endonuclease domain (15,21). MARF1 can physically interact with the mRNA decapping machinery, including EDC4, through its C-terminal region (16,21). However, in contrast to its canonical role in promoting the decay of mRNAs, EDC4 inhibits MARF1-mediated mRNA decay by preventing MARF1 from binding to its targets (15). Still, the mode by which EDC4 interacts with MARF1 and how this interaction inhibits MARF1-mRNA targeting is not known.

In this study, we investigate how EDC4 interacts with MARF1 and the mechanism by which this interaction regulates MARF1-mediated mRNA decay. We show that MARF1 interacts with EDC4 using a conserved EDC4-binding motif (EBM) first identified in the human XRN1 exonuclease. In keeping with this, we show that MARF1 and XRN1 interact with EDC4 in a mutually exclusive manner. Moreover, while the EDC4–MARF1 interaction represses MARF1 activity, we go on to show that association alone is not sufficient. Importantly, we demonstrate that P-body architecture directly prevents MARF1 from mediating the decay of targeted mRNAs. Taken together, our data uncover an unprecedented role for P-bodies in regulating MARF1-mediated mRNA decay, indicating that P-bodies can directly regulate the stability of select mRNA populations in human cells.

## MATERIALS AND METHODS

### Cell lines, cell culture and transfections

Epithelioid carcinoma HeLa cells and human embryonic kidney (HEK) 293T cells lines were obtained from ATCC. Cell lines identities were established via morphology but have not been authenticated and all cells were tested negative for mycoplasma contamination. HEK 293T and HeLa cells were grown in Dulbecco's modified Eagle's medium (DMEM) supplemented with 10% fetal bovine serum, 50 U/ml penicillin and 50 µg/ml streptomycin. RNAi and 3xFLAG-LSM14A complementation cell lines were generated as previously described (7). EDC4-V5 stable cell lines were generated with VSV-G pseudotyped pLENTI6-EDC4-V5 lentiviruses and selected in media containing 10 µg/ml blasticidin. Plasmid transfections were performed using polyethyleneimine (PEI).

### Plasmids and antibodies

Plasmids of pCI-λNHA and pcDNA3 FLAG encoding annotated protein coding sequences were generated by conventional molecular cloning techniques. Point and deletion mutations within the coding sequence of MARF1 were made through site-directed mutagenesis with Phusion DNA polymerase. Similarly, Renilla luciferase (RL) reporter plasmids containing the MAML1 3'UTR region were generated through conventional cloning as described in Broth-

ers *et al.* 2020 (15). V5-tagged EDC4 proteins were generated by Gateway cloning from pDONR-EDC4 regions into pDEST40 vectors (ThermoFisher). Antibodies for this study were purchased against HA (Covance), FLAG (Sigma), V5 (Rabbit - Cell Signaling; Mouse - ThermoFisher), EDC4 (Bethyl), DDX6 (Bethyl), and XRN1 (Bethyl). Antibodies used in western blot and immunofluorescence microscopy analyses were diluted to the manufacturer's specifications for each application.

### Luciferase reporter assays

HeLa cells were seeded at a density of ~30% confluency and transfected with plasmids encoding for the indicated proteins with RL-MAML1 3'UTR and FL (control) plasmids 24 h post-seeding. After an additional 24 h post-transfection, cells were harvested and lysed in Passive Lysis Buffer (Promega). The activity levels of the Renilla (RL) and firefly (FL) luciferase was measured using a Dual-Luciferase Assay (Promega). Cell lysates were also analyzed by western blotting to determine relative protein expression levels.

### mRNA stability assays

To assess *RL-MAML1* mRNA decay, HeLa cells were transfected with plasmids encoding the indicated proteins along with one encoding RL-MAML1. Forty-eight hours post-transfection, cell culture media was replaced with media containing actinomycin D (5 µg/ml). Cells were harvested at the indicated timepoints, pelleted and flash frozen before being stored at –80°C. Frozen pellets were processed for RT-qPCR as described below.

### RT-qPCR assays

To assess relative steady-state mRNA levels, HeLa cells were co-transfected with MARF1 variants and an empty puromycin-resistance selection cassette 24 h post-seeding. Twenty-four hours post-transfection, the cell culture media was replaced with complete cell culture media containing 2 µg/ml of puromycin. Following 24 h of puromycin selection, cells were harvested, and RNA was extracted using EZ-10 Spin Column RNA Miniprep Kit (Biobasic). Extracted RNA was treated with Turbo DNase (Invitrogen) for 1 h at 37°C and inactivated with Inactivation Buffer (Invitrogen). Purified RNA was quantified using a Nanodrop and 250 ng was random hexamer-primed and reverse transcribed following the protocol for Maxima H Minus Reverse Transcriptase (ThermoFisher). Quantitative PCR was carried out with GoTaq qPCR Master Mix (Promega), 5 µl of 1:3 diluted cDNA, and primers (IDT) against the coding sequence of endogenous *GAPDH* (control) and *MAML1* mRNAs. Primers for mRNA decay assays were against *GAPDH* (control) and Renilla luciferase (RL). Reactions were carried out on an Eppendorf realplex2 thermocycler and conditions entailed an initial step of 95°C for 2min, followed by 40 cycles of 95°C for 15 s, 55°C for 15 s and 68°C for 20 s. Finally, a melting curve was performed by incubating samples at 60°C for 15 s followed by a temperature gradient increase to 95°C over 20 min. Samples were measured

for two technical replicates with mean CT values being analyzed for three biological replicates. To ensure no DNA contamination, no-reverse transcriptase controls were performed. Normalized mRNA levels were calculated by taking the experimental sample CT (*MAMLI* or *RL-MAMLI*) and subtracting the CT of the *GAPDH* control to generate  $\Delta$ CT values. For steady-state qPCR experiments, the  $\Delta$ CT of MARF1<sup>ΔNYN</sup> was subtracted from each sample to generate  $\Delta\Delta$ CT for each condition. For mRNA decay experiments, the  $\Delta$ CT at timepoint zero was subtracted from each timepoint to generate  $\Delta\Delta$ CT for each sample and timepoint. Relative mRNA levels were calculated as  $2^{-\Delta\Delta$ CT}.

### Immunofluorescence staining

Indicated cells were seeded on coverslips for 24 h, and subsequently transfected with plasmids encoding the indicated proteins. Twenty-four hours post-transfection, cells were washed twice with PBS and then subsequently fixed with 4% formaldehyde in PBS for 20 min. After formaldehyde fixing, cells were washed four times with PBS and then permeabilized with 0.1% triton X-100 in PBS (PBS-T) for 20 min. After permeabilization, coverslips were blocked in 4% bovine serum albumin (BSA) in PBS at room temperature (RT) for 1 h. Indicated primary antibodies were diluted 1:500 in 4% BSA. Diluted antibodies were added to the coverslips after blocking and left to incubate at 4°C overnight. The next day, cells were washed three times with PBS-T. Secondary anti-bodies were diluted 1:500 for both Alexa Fluor 488 goat anti-rabbit and Alexa Fluor 594 goat anti-mouse in 4% BSA (ThermoFisher). Secondary antibody was added to the coverslips and incubated at RT for 45 min, shielded from light. Post-secondary incubation, coverslips were washed once with PBS-T and then three additional times with PBS to remove any residual triton. Nuclei were stained with DAPI for 15 min at RT, shielded from light. Coverslips were washed four times with PBS before being mounted on to glass slides with ProLong Gold media (ThermoFisher). Images were taken using a Zeiss Confocal LSM 800 microscope at 40× magnification and processed with ImageJ to merge channels and add scale bars.

### Co-immunoprecipitation assays

Indicated cell lines were plated in 10 cm dishes and transfected with plasmids encoding the indicated proteins. Forty-eight hours after transfection, cells were harvested and lysed in lysis buffer (50 mM Tris-HCl, pH 7.4; 150 mM NaCl; 0.5% NP40 (Igepal CA630); 2 mM EDTA; 1 mM DTT; 1U benzonase; protease inhibitors; in water). Lysates were clarified by centrifugation at 15 000 g and diluted to 2 mg/ml. Lysates were then pre-cleared with 30 μl of packed Protein G Agarose Fast Flow (Millipore) for 45 min at 4°C with end-over-end rotation. For FLAG immunoprecipitation experiments, pre-cleared lysates were incubated with 25 μl of packed FLAG M2 agarose beads (Sigma-Aldrich) (or Protein G Agarose Fast Flow beads as control) and incubated for 3 h at 4°C with end-over-end rotation. For V5 immunoprecipitation experiments, pre-cleared lysates were incubated with 2 μg of V5 antibody (Cell Signaling) (or no

antibody as control) overnight at 4°C with end-over-end rotation. The following day, lysates were incubated with 30 μl packed Protein G Agarose Fast Flow (Millipore) for 2 h at 4°C with end-over-end rotation. For both FLAG and V5 IP experiments, beads were washed five times with 1 ml of cold lysis buffer and eluted by boiling beads in 40 μl 1× SDS-PAGE sample buffer. Input and immunoprecipitation samples were then analyzed by western blotting.

### RNA immunoprecipitation assays

HeLa cells were plated in 10 cm dishes and transfected with plasmids encoding FLAG-MARF1<sup>ΔNYN</sup> and either GFP (control) or V5-tagged EDC4<sup>WT</sup> / EDC4<sup>ΔDistal</sup>. Forty-eight hours after transfection, cells were harvested and lysed in lysis buffer (50 mM Tris-HCl, pH 7.4; 150 mM NaCl; 0.5% NP40 (Igepal CA630); 2 mM EDTA; protease and RNase inhibitors; in RNase-free water). 1.5 mL of lysate was split into halves, with one half getting FLAG-coupled DynaBeads™ and the other getting DynaBeads™ alone for a 2 h immunoprecipitation at 4°C with end-over-end rotation. Aliquots were taken for RNA and Protein inputs. Beads were then magnetized and stringently washed with 4 × 1 ml lysis buffer. 20% of the washed beads were taken for validation by western blot with the 'Protein Input' samples. The remaining beads were incubated with RLT buffer (Qiagen), magnetized, and RNA was extracted using the Qiagen RNeasy mini kit. Extracted RNA levels were quantified by RT-qPCR, as described above. To measure MARF1-target mRNA enrichment levels, the input and immunoprecipitation samples were analyzed separately. The CT values of the *MAMLI* mRNA as determined by qPCR were first normalized to the *GAPDH* mRNA CT values ( $\Delta$ CT). This  $\Delta$ CT value for the FLAG immunoprecipitation samples was then normalized to the  $\Delta$ CT value of the control uncoupled bead samples ( $\Delta\Delta$ CT). Finally, the relative fold-change of the  $\Delta\Delta$ CT value was determined by calculating  $2^{-\Delta\Delta$ CT}. After the relative fold-changes were calculated for both input and immunoprecipitation samples, the enrichment in the immunoprecipitation samples was determined by dividing the immunoprecipitation relative fold-change values by the corresponding input relative fold-change values.

## RESULTS

### MARF1 contains an evolutionarily conserved EDC4-binding motif

MARF1 interacts with the mRNA decapping complex, including EDC4, via its C-terminal region (residues 1557-C) (Figure 1A) (15,21). To gain insight into how this region interacts with EDC4, we carried out a comparative sequence analysis of MARF1 orthologs to identify evolutionarily conserved sequences in their C-termini. Sequence alignments reveal two highly conserved stretches of amino acids in the MARF1 C-terminal region; residues 1609–1653 and 1714–1733 (Supplementary Figure S1A). As EDC4 inhibits MARF1-mediated mRNA decay (15), we set out to determine whether deleting either of these stretches within the MARF1 C-terminus prevents EDC4

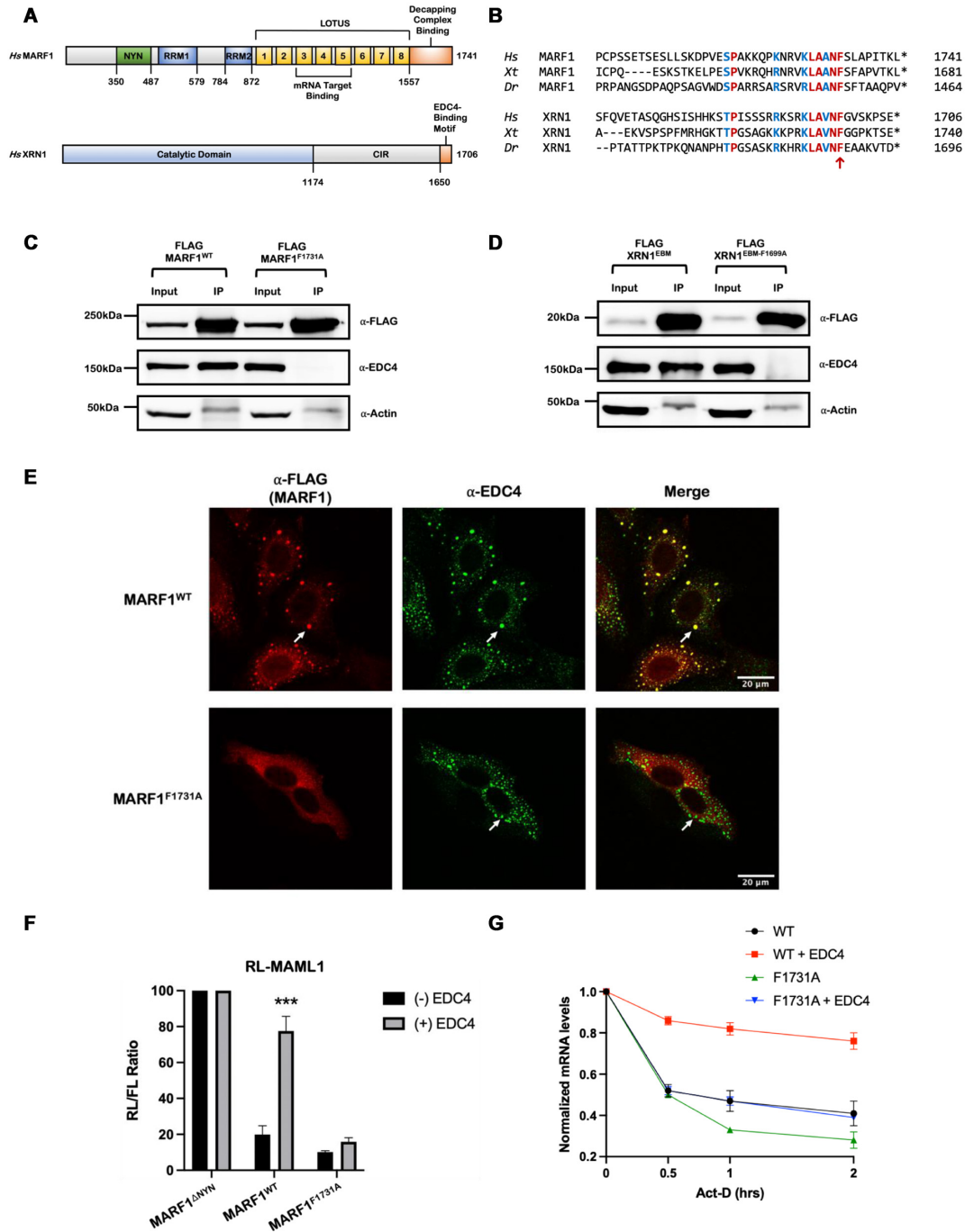


**Figure 1.** MARF1 and XRN1 use analogous motifs to interact with EDC4. (A) Schematic diagram for MARF1 and XRN1 domain structures. (B) Phylogenetic alignment of the candidate C-terminal distal region that mediates MARF1-EDC4 interactions and the XRN1 EDC4-binding motif (EBM) in *H. sapiens* (*Hs*), *X. tropicalis* (*Xt*), and *D. rerio* (*Dr*). Residues in blue are conservative substitutions that are analogous in both proteins, residues in red are identical residues between all orthologs for each protein. The (\*) represents the C-terminus of the protein and an analogous phenylalanine is indicated with a red arrow located within the SLiM; LAΦNF. (C and D) Co-immunoprecipitation experiments performed by incubating HeLa cell extracts expressing the indicated FLAG-tagged proteins and incubated with FLAG antibody. Subsequent western blot analysis was performed to identify the presence of endogenous EDC4. (E) Images generated through confocal microscopy of immunofluorescent staining of HeLa cells transfected with FLAG-MARF1 variants. The merged image represents the overlap of the α-FLAG (red) and α-EDC4 (green) signals and scale bars represent 20 μm. White arrows represent P-bodies as defined by foci with strong signal overlap between red and green staining. (F) RL-MAML1 activity detected in extracts of transfected HeLa cells expressing the annotated proteins and FL as a transfection normalization control. Histograms represent the mean RL activity detected from three biological replicates, normalized to FL activity and the RL/FL ratio of a catalytically inactive MARF1 (MARF1<sup>ΔNYN</sup>) set to 100. Error bars represent the SEM and statistical significance was calculated using a two-tailed T-test comparing RL activity in the (+) to (-) EDC4 overexpression samples (\*\*\**P* < 0.001). (G) The stability of RL-MAML1 was assessed by using actinomycin D (5 μg/ml) for the indicated amount of time in HeLa cells expressing the indicated proteins. Total RNA was isolated, reverse transcribed and RL-MAML1 RNA was quantified by qPCR. RL-MAML1 mRNA decay rates were normalized to *GAPDH* mRNA levels with the zero time point set at 1.0. Error bars represent the SEM for three biological replicates.

from antagonizing MARF1 activity. To test this, we co-transfected HeLa cells with a plasmid encoding EDC4 along with plasmids expressing either wild-type MARF1 (MARF1<sup>WT</sup>) or MARF1 deletion mutants for each conserved region (MARF1<sup>Δ1609–1653</sup> and MARF1<sup>Δ1714–1733</sup>, respectively) (Supplementary Figure S1B). These proteins were expressed along with a *Renilla* luciferase reporter mRNA containing the 3'UTR of *MAMLI*, a *bona fide* MARF1 target (RL-MAMLI). As previously reported (15), MARF1<sup>WT</sup> efficiently represses the RL-MAMLI reporter as compared to a MARF1 mutant lacking its NYN endonuclease domain (MARF1<sup>ΔNYN</sup>) and overexpressing EDC4 antagonizes MARF1<sup>WT</sup> activity (Supplementary Figure S1C–E). EDC4 overexpression similarly inhibits the ability of MARF1<sup>Δ1609–1653</sup> to repress RL-MAMLI; however, MARF1<sup>Δ1714–1733</sup> silences the RL-MAMLI reporter mRNA irrespective of whether EDC4 is overexpressed. These data suggest that the MARF1 C-terminal residues from 1714–1733 are required for EDC4 to antagonize MARF1 activity.

Next, we expanded our sequence analysis of the MARF1 C-terminal region to determine if it shares sequence similarities to other proteins that play a role in mRNA turnover. Interestingly, we observe that the stretch of amino acids in MARF1 that are required for EDC4 to regulate its activity displays strong similarity to a region in the XRN1 exonuclease that directly interacts with EDC4 (Figure 1B) (2,3). This includes a highly conserved aromatic residue (XRN1 F1699 and MARF1 F1731, respectively) within analogous short linear motifs (SLiM); LAΦNF. We set out to determine if the conserved phenylalanine within this SLiM plays a role in establishing an interaction between each ribonuclease and EDC4 using co-immunoprecipitation experiments. Briefly, HeLa cells were transfected with plasmids encoding FLAG-tagged MARF1<sup>WT</sup> or a MARF1 mutant where F1731 was mutated to alanine (MARF1<sup>F1731A</sup>), lysates were incubated with FLAG antibody to precipitate FLAG-MARF1 proteins and analyzed by western blotting. While MARF1<sup>WT</sup> efficiently co-precipitates endogenous EDC4, MARF1<sup>F1731A</sup> does not (Figure 1C). We carried out similar co-immunoprecipitation experiments using a FLAG-tagged XRN1 EDC4-binding motif (XRN1<sup>EBM</sup>; residues 1650–C) (Figure 1A). Like MARF1, mutating the analogous phenylalanine to alanine in the XRN1<sup>EBM</sup> (F1699A) also disrupts its ability to interact with EDC4 (Figure 1D). In agreement with these data, MARF1<sup>F1731A</sup> fails to co-localize with EDC4 and instead displays diffuse staining in the cytoplasm (Figure 1E). This contrasts with MARF1<sup>WT</sup> which co-localizes with EDC4 in P-bodies (16,17). Taken together, these data indicate that MARF1 and XRN1 contain analogous EBM motifs that facilitate their respective interactions with EDC4.

We next evaluated if this central phenylalanine in MARF1 is required for EDC4 to inhibit MARF1 activity. Just as MARF1<sup>Δ1714–1733</sup> represses the RL-MAMLI reporter irrespective of EDC4 overexpression (Supplementary Figure S1C), so too does MARF1<sup>F1731A</sup> (Figure 1F). Consistent with our previously published work (15), this repression was at the level of mRNA decay, where both MARF1<sup>WT</sup> and MARF1<sup>F1731A</sup> promote the

decay of *RL-MAMLI* mRNAs, as assessed by qPCR levels after inhibiting transcription with Actinomycin D (Figure 1G and Supplementary Figure S2A). However, only MARF1<sup>WT</sup>-mediated mRNA decay is inhibited by EDC4-overexpression. Collectively, these data show that the central phenylalanine within the MARF1 C-terminal SLiM is required for MARF1 to interact with EDC4 and for EDC4 to inhibit MARF1-mediated mRNA decay.

### MARF1 and XRN1 ribonucleases interact with EDC4 in a mutually exclusive manner

XRN1 has been reported to bind to the C-terminal α-helical region of EDC4 (2). As both MARF1 and XRN1 use analogous EBMs to interact with EDC4, we next set out to investigate whether MARF1 also interacts with the same region of EDC4 as XRN1 does. To test this, HeLa cells were co-transfected with plasmids encoding FLAG-tagged MARF1 and V5-tagged fragments of EDC4 spanning the entire length of the protein (Figure 2A). Cell lysates were subsequently incubated with FLAG-antibody to precipitate MARF1 protein complexes, which were analyzed by western blotting (Figures 2B and Supplementary Figure S2B). V5-tagged EDC4 fragments containing the N-terminal WD40 domain or the central serine-rich linker region fail to co-precipitate with FLAG-tagged MARF1. In contrast, the C-terminal region of EDC4 (974–1401), which harbors a large α-helical region, interacts with MARF1 as well as full-length EDC4. The C-terminal α-helical region of EDC4 contains two α-helices; the proximal and the distal helical regions (Figure 2A). We observe that EDC4 lacking the proximal helix (EDC4<sup>ΔProximal</sup>) fails to interact with MARF1, whereas an EDC4 mutant lacking the distal helical region (EDC4<sup>ΔDistal</sup>) interacts with MARF1 efficiently (Figures 2B and Supplementary Figure S2C). These results are consistent with previous reports that XRN1 also binds to the proximal helix of EDC4 (2,3).

The analogous modes of EDC4 association with MARF1 and XRN1 led us to posit that MARF1 and XRN1 may be interacting with the exact same surface on the EDC4 C-terminal α-helical region. We previously showed that expressing the MARF1 C-terminal region (MARF1<sup>C-term</sup>) enhances full-length MARF1<sup>WT</sup> activity to similar levels when compared to a mutant that cannot interact with endogenous EDC4 by acting as a decoy (Figure 3A) (15). The decoy effect by MARF1<sup>C-term</sup> is only visible in a range where MARF1<sup>WT</sup> is expressed at a low-levels such that in its absence, endogenous EDC4 is sufficient to impair MARF1<sup>WT</sup> activity (Figures 3B; Supplementary Figure S2D and E). However, co-transfecting a MARF1<sup>C-term</sup> harboring a F1731A mutation that abolishes the MARF1-EDC4 interaction fails to enhance MARF1<sup>WT</sup> activity. In keeping with our model that XRN1 and MARF1 interact with EDC4 in a similar manner, expressing the XRN1<sup>EBM</sup> also prevents EDC4 from antagonizing MARF1 activity (Figures 3B, Supplementary Figure S2D and F). In addition, this was dependent upon the ability of the XRN1<sup>EBM</sup> to interact with EDC4, as a XRN1<sup>EBM</sup> harboring the F1699A mutation, which abolishes its interaction with EDC4 fails to enhance the activity of MARF1<sup>WT</sup>. To

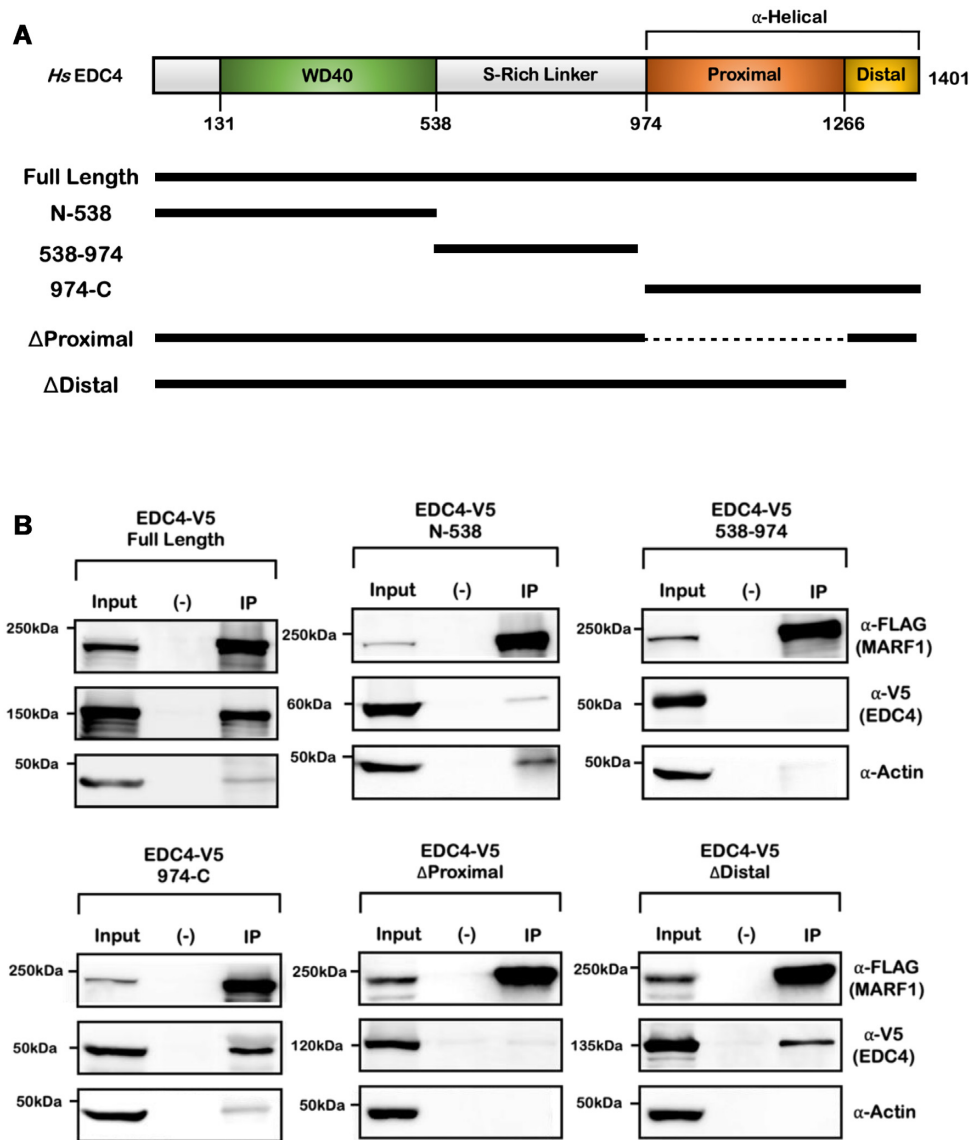


**Figure 2.** MARF1 associates with the C-terminal proximal  $\alpha$ -helix within EDC4. (A) Schematic diagrams of wild-type EDC4, along with the indicated EDC4 protein fragments and their relative positions. (B) Co-immunoprecipitation experiments performed by incubating HeLa cell extracts expressing FLAG-MARF1 and the indicated V5-tagged EDC4 protein fragments. Extracts were incubated with FLAG-antibody and analyzed by western blotting.

determine whether MARF1 and full-length XRN1 directly compete for EDC4, we generated HEK 293T cells that stably express V5-tagged EDC4 and transiently transfected them with plasmid encoding FLAG-tagged MARF1<sup>C-term</sup>. Cell lysates were incubated with V5 antibody to precipitate EDC4 and analyzed by western blotting to assess XRN1 co-precipitation (Figure 3C). Consistent with our hypothesis, expressing the WT MARF1<sup>C-term</sup> dramatically decreases the association of endogenous XRN1 with V5-tagged EDC4 as compared non-transfected cells. In contrast, expressing the MARF1<sup>C-term</sup> mutant that cannot associate with EDC4 (F1731A) fails to impair XRN1 association with EDC4. Collectively, these results suggest that the MARF1 and XRN1 ribonucleases interact with the proximal  $\alpha$ -helical region in EDC4 in a mutually exclusive manner.

#### EDC4-MARF1 interaction is required but not sufficient to inhibit MARF1 activity

EDC4 impairs MARF1-mediated mRNA decay by inhibiting MARF1 from interacting with target mRNAs (15). However, EDC4<sup>ΔProximal</sup>, which does not interact with MARF1 fails to inhibit MARF1 activity when ectopically expressed (Figures 4A, and Supplementary Figure S2C and G). However, we observed that expressing EDC4<sup>ΔDistal</sup>, which efficiently interacts with MARF1 (Figure 2B), also fails to antagonize MARF1 activity (Figures 4A, and Supplementary Figure S2C and G) or prevent MARF1 from binding to a targeted endogenous *MAML1* mRNA, as assessed by RNA-immunoprecipitation (Figure 4B). Taken together, these results suggest that while the EDC4-MARF1 interaction is required for it to regulate

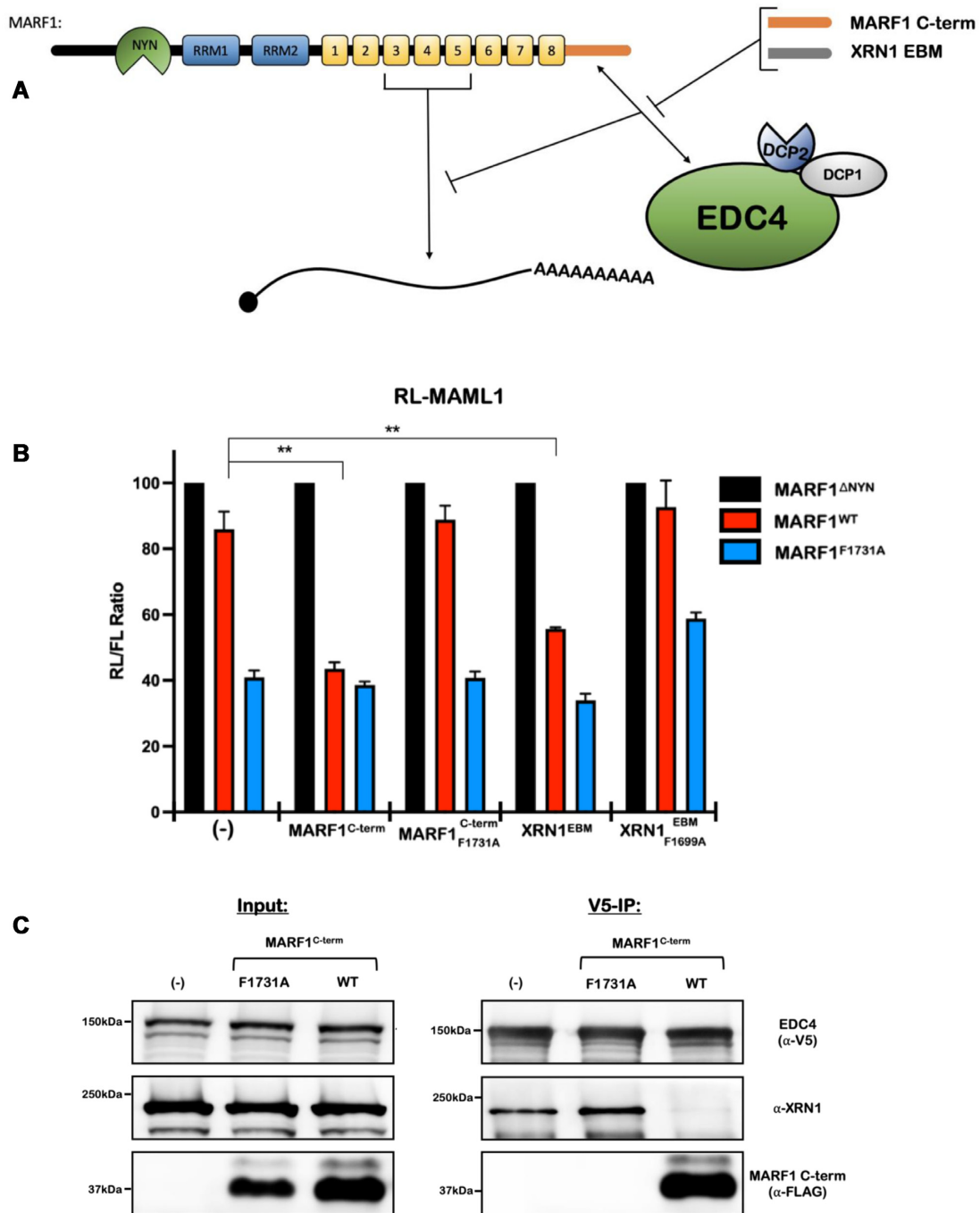


**Figure 3.** MARF1 and XRN1 competitively interact with EDC4 in a mutually exclusive manner. (A) Schematic diagram representing the reporter assay in (B), where the MARF1<sup>C-term</sup> or the XRN1<sup>EBM</sup> compete with low levels of full-length MARF1 for interacting with endogenous EDC4. (B) RL-MAML1 activity detected in extracts of transfected HeLa cells expressing the annotated proteins and FL as a transfection normalization control. Histograms represent the mean RL activity detected from three biological replicates, normalized to FL activity and the RL/FL ratio of a catalytically inactive MARF1 (MARF1<sup>ΔNYN</sup>) set to 100. Error bars represent the SEM and statistical significance was calculated using a two-tailed T-test comparing RL activity to the (-) samples for MARF1<sup>WT</sup> samples (\*\**P* < 0.01). (C) Co-immunoprecipitation experiments performed on HEK 293T cells stably expressing V5-tagged EDC4. Cells were transfected with MARF1 C-term variants and a puromycin selectable marker. Puromycin-selected cell lysates were subsequently incubated with V5-antibody and then analyzed by western blotting for the presence of endogenous XRN1.

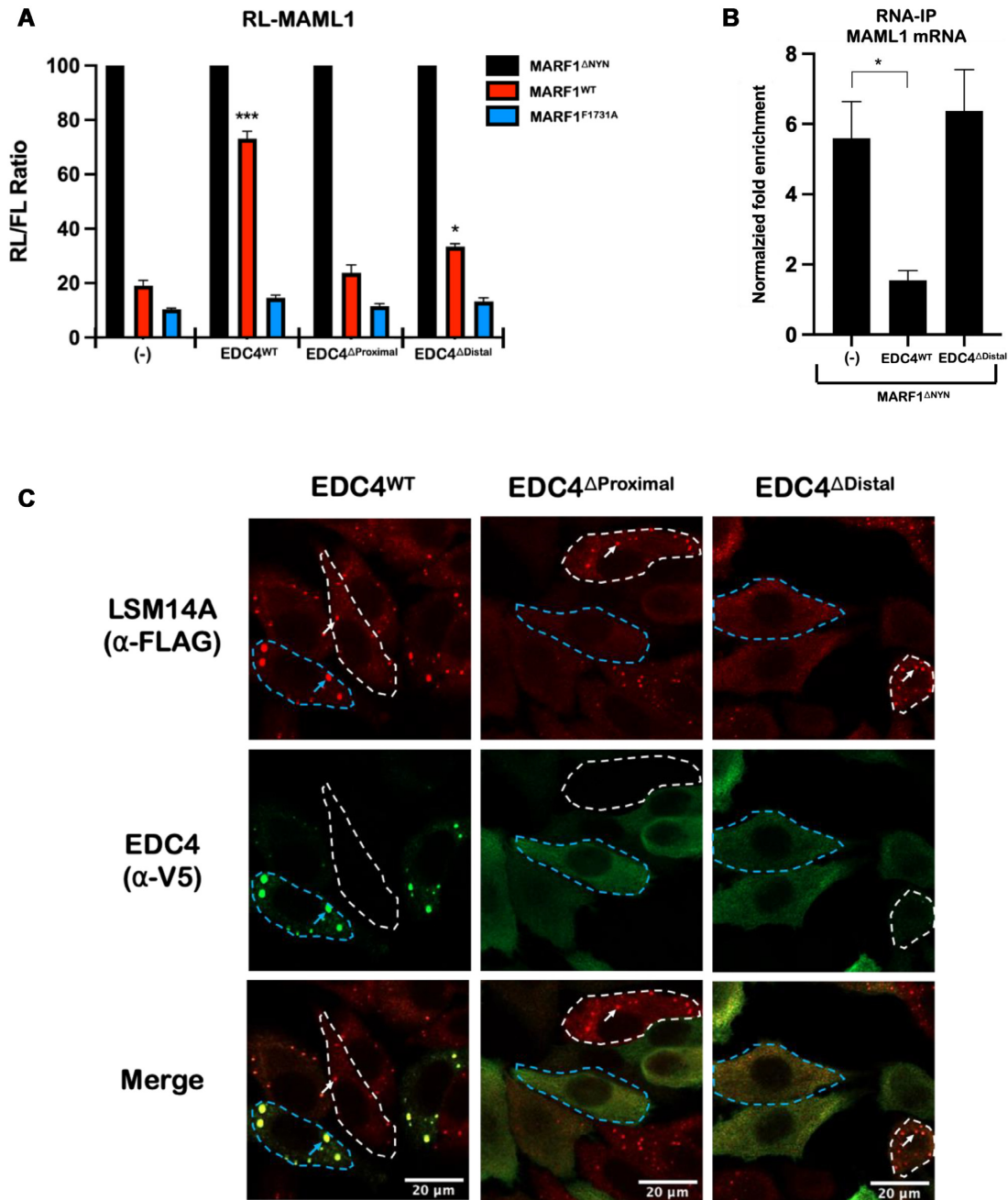


**Figure 4.** EDC4-MARF1 association is necessary but not sufficient to antagonize MARF1 activity. (A) RL-MAML1 activity detected in extracts of transfected HeLa cells expressing the annotated proteins and FL as a transfection normalization control. Histograms represent the mean RL activity detected from three biological replicates, normalized to FL activity and the RL/FL ratio of a catalytically inactive MARF1 (MARF1<sup>ΔNYN</sup>) set to 100. Error bars represent the SEM and statistical significance was calculated using a two-tailed T-test comparing RL activity to the (-) samples for MARF1<sup>WT</sup> samples (\* $P < 0.05$ ; \*\*\* $P < 0.001$ ). (B) RNA-immunoprecipitation (IP) experiments conducted on HeLa cells expressing the indicated proteins. Cell lysates were incubated with FLAG antibody to precipitate FLAG-MARF1<sup>ΔNYN</sup> complexes. RNA was purified from the IP fraction and reverse transcribed. Histograms represent the mean fold-enrichment of *MAML1* mRNA transcripts detected by qPCR in three experiments, normalized to *GAPDH* levels, mock IP controls, and input mRNA levels. Error bars represent the SEM of three biological replicates and statistical significance was calculated using a two-tailed T-test relative to (-) samples (\* $P < 0.05$ ). (C) Images generated through confocal microscopy of immunofluorescent staining of HeLa cells stably expressing FLAG-tagged LSM14A. Cells were transfected with the indicated V5-tagged EDC4 proteins prior to staining. The merged image represents the overlap of the α-FLAG (red) and α-V5 (green) signals and scale bars represent 20 μm. Cells outlined in blue dotted lines represent cells which were transfected to contrast with untransfected cells outlined in dotted white lines. Blue arrows indicate P-bodies present in transfected cells, while white arrows indicate P-bodies present in untransfected cells.

MARF1 activity, this interaction is not sufficient on its own to do so. We therefore set out to determine what, in addition to interacting with MARF1, allows EDC4 to regulate MARF1-mediated mRNA decay. Given that EDC4 localizes to and promotes P-body formation (10) and the distal helix within the *D. melanogaster* EDC4 ortholog has been implicated in P-body localization (22), we set out to determine if deleting the  $\alpha$ -helical domains from EDC4 alters its localization to P-bodies. To test this, HeLa cells stably expressing FLAG-tagged LSM14A (a key P-body marker) were transiently transfected with plasmids encoding V5-tagged EDC4<sup>WT</sup>, EDC4 <sup>$\Delta$ Proximal</sup> or EDC4 <sup>$\Delta$ Distal</sup> (Supplementary Figure S2G), and the localization patterns of these proteins were assessed by immunofluorescence microscopy (Figure 4C). In agreement with both EDC4 and LSM14A being core P-body proteins, we observe V5-EDC4<sup>WT</sup> and FLAG-LSM14A co-localizing to discrete cytoplasmic foci. In contrast, EDC4 <sup>$\Delta$ Proximal</sup> or EDC4 <sup>$\Delta$ Distal</sup> mutants exhibit diffuse staining through the cytoplasm. Strikingly, cells that express these EDC4 helical mutants (outlined in dotted blue lines) fail to form P-bodies, as determined by the diffuse staining pattern of FLAG-LSM14A. This contrasts with untransfected cells (outlined in white dotted lines), where FLAG-LSM14A localizes to punctate foci. The apparent dominant-negative effects of these EDC4  $\alpha$ -helical mutants on P-body formation may be due to the loss of protein-protein interactions that are required for P-body formation, given that this region interacts with multiple P-body proteins (e.g. DCP2 and XRN1) and plays a role in EDC4 oligomerization (2,22). Thus, while our previous data indicate that the EDC4–MARF1 interaction inhibits MARF1-mediated mRNA decay, an EDC4 mutant that interacts with MARF1 but does not support P-body formation fails to inhibit MARF1 activity.

### P-bodies directly inhibit MARF1-mediated mRNA decay

P-bodies are maintained through a complex network of multivalent protein-protein interactions, including interactions between LSM14A with EDC4, DDX6 and 4E-T (7,9,23,24). Given that MARF1 mutants that do not interact with EDC4 also fail to localize to P-bodies (Figures 1C and E) (15,21) and that overexpressing an EDC4 mutant which interacts with MARF1 but inhibits P-body formation fails to inhibit MARF1 activity (Figure 4A–C), we set out to investigate whether P-body architecture plays a direct role in regulating MARF1-mediated mRNA decay. To do so, we took advantage of HeLa cell lines that have been depleted of endogenous LSM14A by RNAi and complemented with either FLAG-tagged LSM14A<sup>WT</sup> or LSM14A mutants that disrupt its contact with 4E-T, EDC4, or DDX6 (LSM14A<sup>Y22E/I29E</sup>, LSM14A <sup>$\Delta$ FFD</sup> or LSM14A <sup>$\Delta$ TFG</sup>, respectively) (Supplementary Figure S3A). Importantly, disrupting LSM14A contact with any of these proteins in cells renders them unable to form microscopically visible P-bodies (Supplementary Figure S3B and C) (7). Ectopically expressed EDC4 co-localizes with FLAG-tagged LSM14A<sup>WT</sup> and endogenous DDX6 in large punctate foci (Figures 5A; Supplementary Figures S4A and S5A). However, EDC4 does not colocalize with LSM14A or DDX6 in LSM14A mutant cells, with all three proteins displaying diffuse cytoplasmic

staining. Consistent with previous data, ectopically expressing EDC4 antagonizes MARF1 activity in cells expressing LSM14A<sup>WT</sup> (Figure 5B). However, overexpressing EDC4 does not robustly inhibit MARF1 activity in LSM14A mutant cells that cannot form P-bodies (Figures 5C through E). These results were recapitulated in the context of endogenous MARF1 targets, where steady-state levels of endogenous *MAML1* mRNA in cells expressing MARF1<sup>WT</sup> are elevated by ectopic EDC4 expression in LSM14A<sup>WT</sup> cells but not in the LSM14A <sup>$\Delta$ FFD</sup> cell line (Figures 5F and G).

Establishing causal roles for P-bodies in regulating mRNA decay has remained elusive due to the confounding effects of central P-body members also exhibiting granule-independent roles in regulating mRNA decay (24–26). Therefore, to modulate visible P-bodies without mutating or altering the levels of endogenous P-body proteins, we transiently transfected cells with a plasmid encoding FLAG-tagged NBDY, a microprotein that ablates P-body formation when expressed (27–29). In agreement with previous reports, NBDY expression impairs visible P-body formation, with EDC4 and DDX6 exhibiting diffuse cytoplasmic staining in NBDY-expressing cells (Figure 6A and Supplementary Figure S5B). Moreover, overexpressing NBDY prevents EDC4 from inhibiting MARF1-mediated mRNA decay (Figure 6B–C and Supplementary Figure S2A).

While our data suggest that P-body formation directly inhibits MARF1-mediated mRNA decay, this was always in the context of EDC4-overexpression. Therefore, we set out to determine if endogenous P-bodies alter MARF1-mediated mRNA decay in the absence of EDC4-overexpression. To this end, we transfected LSM14A<sup>WT</sup> or P-body deficient LSM14A mutant cell lines with a plasmid encoding RL-MAML1, as well as low amounts of a MARF1-expressing plasmids such that the level of expression was sufficiently low enough for endogenous EDC4 to impair MARF1<sup>WT</sup> activity relative to a mutant that cannot interact with EDC4 (MARF1<sup>F1731A</sup>) (Figure 3B and Supplementary Figure S2D). Interestingly, in contrast to LSM14A<sup>WT</sup> cells (Figure 6D), low levels of MARF1<sup>WT</sup> efficiently repressed RL-MAML1 reporter levels in cells expressing LSM14A mutants that do not form visible P-bodies (Figure 6E–G and Supplementary Figure S3B). These results support a model where P-body integrity is required for EDC4 to inhibit MARF1 activity and disrupting P-bodies has the potential to enhance MARF1-mediated mRNA decay. Taken together, these data demonstrate that P-bodies can play a causal role in regulating whether the MARF1 endonuclease can interface with and promote the decay of targeted mRNAs.

## DISCUSSION

In this study, we provide functional and mechanistic insights into how the MARF1 endoribonuclease interacts with the enhancer of mRNA decapping EDC4, and how these interactions regulate MARF1-mediated mRNA decay. Importantly, our data point to P-bodies playing a direct role in regulating MARF1-mediated mRNA decay. Taken together, our results indicate that P-bodies use EDC4 to sequester MARF1, rendering MARF1 unable to interact with and degrade targeted mRNAs (Figure 7).

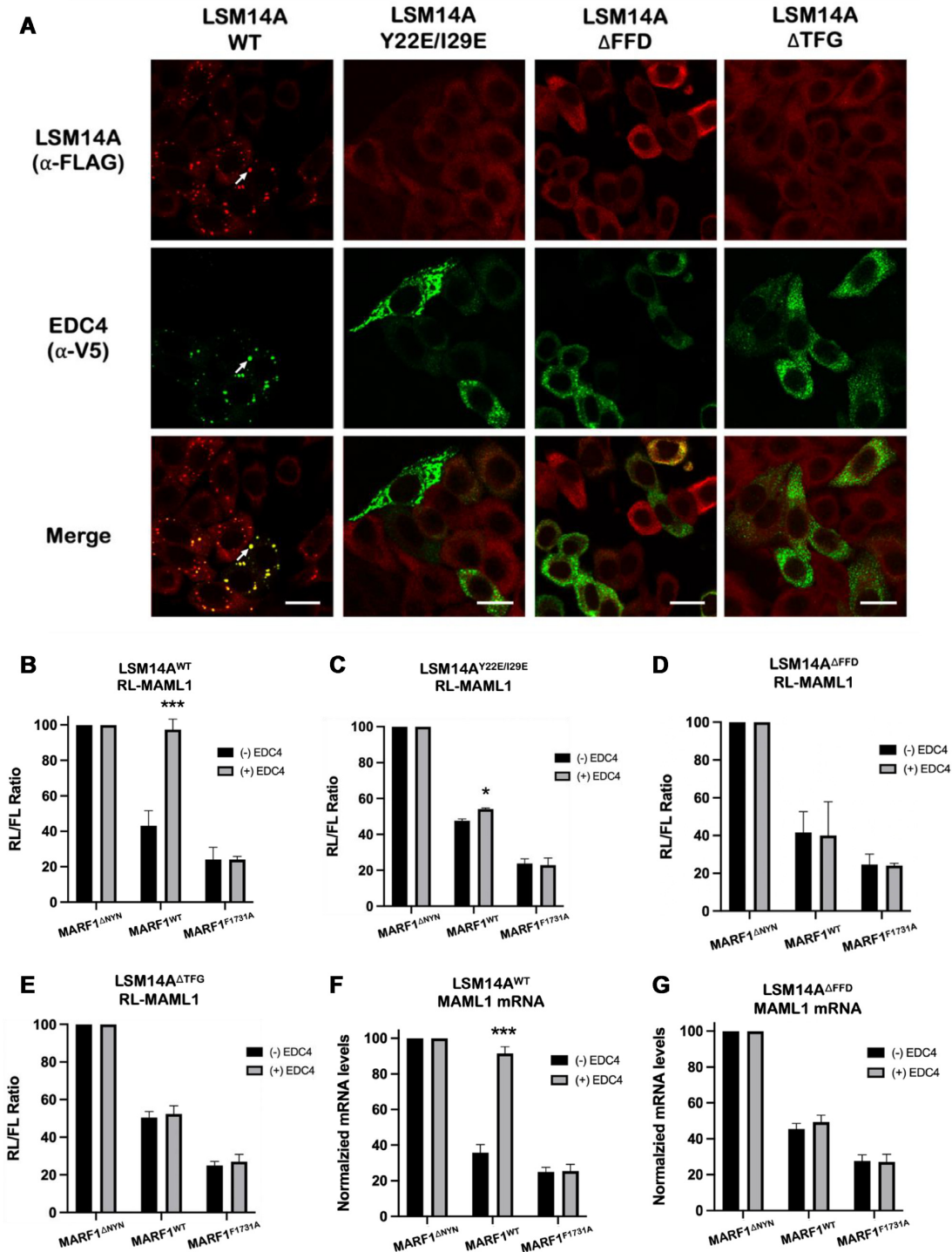


**Figure 5.** EDC4 requires P-bodies to negatively regulate MARF1 activity. (A) Images generated through confocal microscopy of immunofluorescent staining of HeLa cells stably expressing FLAG-tagged LSM14A variants as indicated. Cells were transfected with V5-tagged EDC4 prior to staining. The merged image represents the overlap of the  $\alpha$ -FLAG (red) and  $\alpha$ -V5 (green) signals and scale bars represent 20  $\mu$ m. White arrows indicate P-bodies as defined by intense signal overlap between red and green staining. (B–E) RL-MAML1 activity detected in extracts of HeLa cells that have been supplemented with either FLAG-LSM14A<sup>WT</sup> (B) or the indicated FLAG-LSM14A mutants (C–E). Cells were transfected with plasmids encoding the annotated proteins and FL as a transfection normalization control. Histograms represent the mean RL activity detected from three biological replicates, normalized to FL activity and the RL/FL ratio of a catalytically inactive MARF1 (MARF1 <sup>$\Delta$ NYN</sup>) set to 100. Error bars represent the SEM and statistical significance was calculated using a two-tailed T-test comparing RL activity in the (+) to (-) EDC4 overexpression samples (\* $P$  < 0.05; \*\*\* $P$  < 0.001). (F and G) Endogenous steady-state *MAML1* mRNA levels detected in LSM14A-complemented HeLa extracts expressing the indicated proteins. Histograms represent the mean *MAML1* mRNA levels normalized to *GAPDH* mRNA levels for three biological replicates, where normalized *MAML1* mRNA levels in cells expressing the catalytically inactive MARF1 (MARF1 <sup>$\Delta$ NYN</sup>) are set to 100. Error bars represent the SEM and statistical significance was calculated using a two-tailed T-test comparing RL activity in the (+) to (-) EDC4 overexpression samples (\*\*\* $P$  < 0.001).

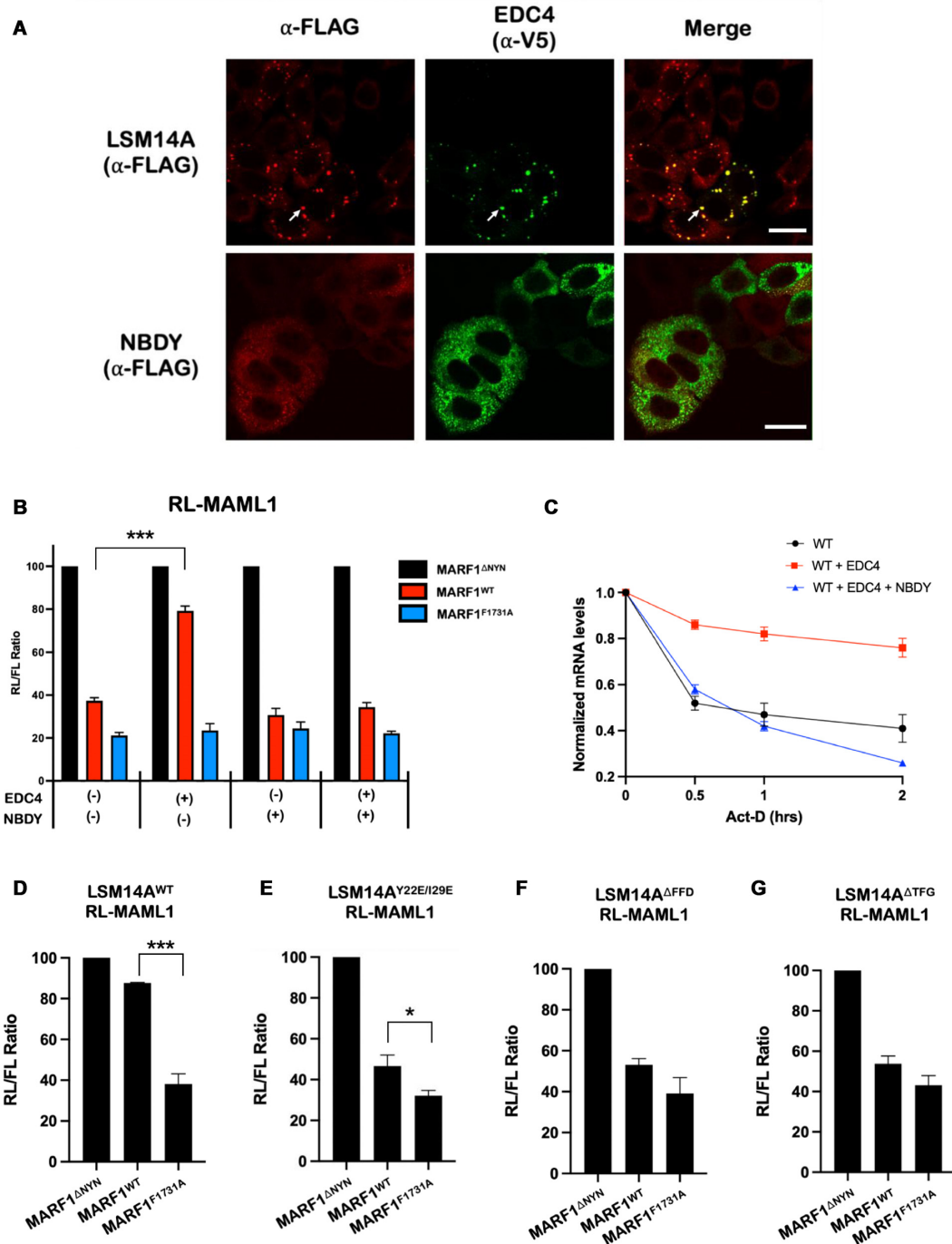


**Figure 6.** P-body dynamics directly regulate MARF1 activity. (A) Images generated through confocal microscopy of immunofluorescent staining of either cells stably expressing FLAG-tagged LSM14A (top) or WT HeLa cells (bottom). Cells were transfected with V5-tagged EDC4 (and FLAG-tagged NBDY for bottom images) prior to staining. The merged image represents the overlap of the  $\alpha$ -FLAG (red) and  $\alpha$ -V5 (green) signals and scale bars represent 20  $\mu$ m. White arrows represent P-bodies as defined by foci with strong signal overlap between red and green staining. (B) RL-MAML1 activity detected in extracts of transfected HeLa cells expressing the annotated proteins and FL as a transfection normalization control. Histograms represent the mean RL activity detected from three biological replicates, normalized to FL activity and the RL/FL ratio of a catalytically inactive MARF1 (MARF1<sup>ΔNYN</sup>) set to 100. Error bars represent SEM and statistical significance was calculated using a two-tailed T-test comparing RL activity to the (-) samples (\*\**P* < 0.001). (C) The stability of RL-MAML1 was assessed by using actinomycin D (5  $\mu$ g/ml) for the indicated amount of time in HeLa cells expressing the indicated proteins. Total RNA was isolated, reverse transcribed and RL-MAML1 RNA was quantified by qPCR. RL-MAML1 mRNA decay rates were normalized to *GAPDH* mRNA levels with the zero time point set at 1.0. Error bars represent the SEM for three biological replicates. (D–G) RL-MAML1 activity detected in extracts of HeLa cells that have been supplemented with either FLAG-LSM14A<sup>WT</sup> (C) or the indicated FLAG-LSM14A mutants (D–F). Cells were transfected with plasmids encoding the annotated proteins and FL as a transfection normalization control. Histograms represent the mean RL activity detected from three biological replicates, normalized to FL activity and the RL/FL ratio of a catalytically inactive MARF1 (MARF1<sup>ΔNYN</sup>) set to 100. Error bars represent SEM of biological replicates and statistical significance was calculated using a two-tailed T-test comparing RL activity between the MARF1<sup>WT</sup> and MARF1<sup>F1731A</sup> samples (\**P* < 0.05; \*\*\**P* < 0.001).

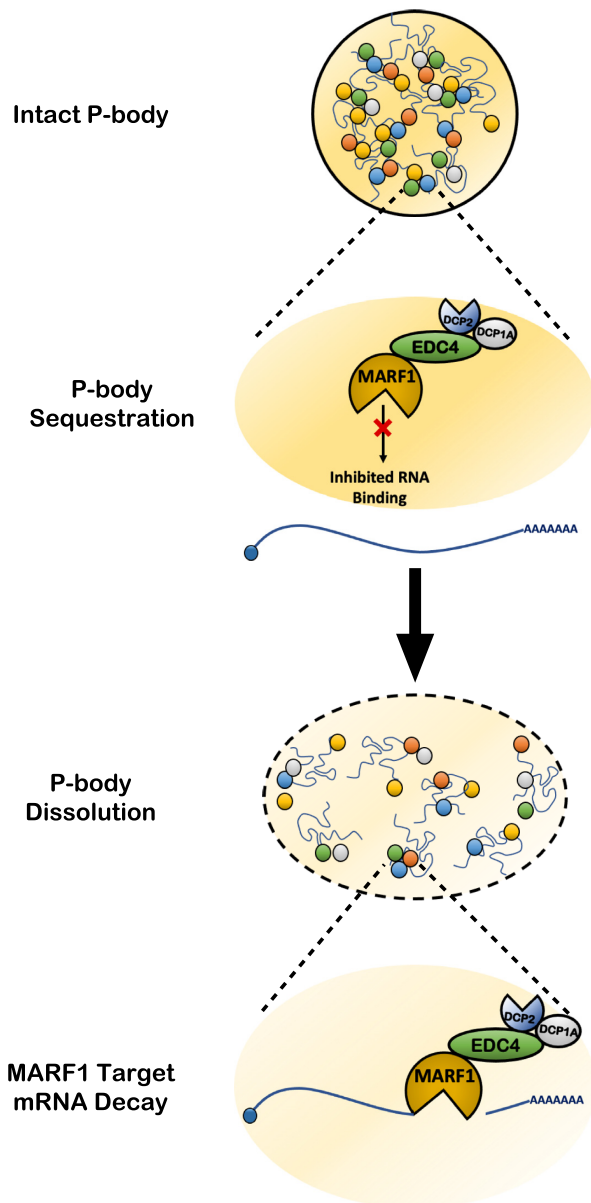


**Figure 7.** Model for how P-body architecture regulates MARF1-mediated mRNA decay. In the presence of intact P-bodies, the MARF1–EDC4 interaction leads to the sequestration of MARF1 to P-bodies in a way that inhibits its RNA-binding and mRNA decay potential. By ablating endogenous P-bodies, MARF1 exists in an active form that can robustly decay target mRNAs.

#### EDC4 interacts with a conserved SLiM shared by the MARF1 and XRN1 ribonucleases

The efficient assembly of the mRNA decapping complex is mediated through EDC4, which helps facilitate efficient mRNA decapping *in vivo* (2,13). EDC4 acts, in part, as a scaffold protein to bridge the interaction of the DCP2 decapping enzyme with DCP1A. This interaction is required *in vitro* to mediate the hydrolysis of the N<sup>7</sup>-methylguanosine cap on the 5' end of the mRNA (2). The cleavage of the 5' cap facilitates subsequent 5'-3' mRNA decay through the XRN1 ribonuclease, which directly contacts EDC4 in

humans (2,3). In addition to the mRNA decapping and decay factors that comprise the canonical mRNA decapping complex, MARF1 also physically interacts with EDC4 in cells (16,21). With the exception of DCP1A—which interacts with the N-terminal WD40 domain of EDC4—the aforementioned mRNA decay factors (DCP2, XRN1 and MARF1) all interact with the C-terminal  $\alpha$ -helical region of EDC4 (2). While no direct interaction between MARF1 and EDC4 has been established, we show here that MARF1 and XRN1 interact with EDC4 in human cells using analogous motifs, which contain a SLiM (LA $\Phi$ NF) that is conserved in both ribonucleases across vertebrates. In *D. melanogaster*, XRN1 does not maintain an obvious EBM and instead associates with the mRNA decapping complex through a direct interaction with DCP1 (3). Similarly, the MARF1 ortholog within *D. melanogaster* does not contain an EBM. This ortholog has significantly diverged from other MARF1 proteins, where it does not contain a NYN endonuclease domain and, rather than interacting with the mRNA decapping complex, it interacts with the CCR4-NOT deadenylation machinery through its first LOTUS domain (30).

Several proteins that interact with core P-body components do so using conserved binding motifs. For example, EDC3, LSM14A and Pat proteins use a conserved FDF motif to bind DDX6 in a mutually exclusive manner (24). Similarly, our data indicate that MARF1 and XRN1 also use a SLiM to interact with EDC4 in a mutually exclusive manner. Nevertheless, whether MARF1 and XRN1 ever compete for EDC4 under normal cellular conditions is less clear. MARF1 is typically expressed at low levels in somatic cells as compared to robust expression in the early stages of oogenesis (20,31). Moreover, most mRNAs remain unusually stable during oogenesis, where deadenylation is uncoupled from mRNA decapping (32). Indeed, *Dcp1a* and *Dcp2* transcripts remain dormant in mouse oocytes until the oocyte-to-zygote transition where they facilitate a wave of maternal mRNA destabilization by reactivating the 5'-3' decay pathway (33). Thus, it is possible that differing biologically relevant contexts for MARF1 and XRN1 preclude the competitive interaction for EDC4 *in vivo*.

#### P-body architecture directly regulates MARF1-mediated mRNA decay

While widely reported from yeast to human cells, P-bodies remain enigmatic. P-bodies have been reported to contain translationally repressed mRNAs, however despite containing an array of factors involved in mRNA decay, mRNAs enriched within P-bodies do not appear to be actively undergoing decay (12). While the composition and structure of P-bodies have been the subject of study for quite some time, it has not been until recently that direct roles for P-bodies in regulating mRNAs have been described. For instance, disrupting P-bodies in embryonic stem cells through knocking down *DDX6* or *LSM14A* releases mRNAs that code for transcription and chromatin remodeling factors that are subsequently translated and impact cell fate (25). In *D. melanogaster*, it has recently been reported that P-bodies can regulate early development—through the sequestration of the *bicoid* mRNAs (34)—and intestinal stem cell iden-

tity through the repression of pro-differentiation transcripts (35). To date, described roles for P-bodies in regulating the transcriptome have been exclusively through translationally repressing the mRNAs that localize to P-bodies. In contrast to these observations, here we report a novel role for P-bodies in directly regulating the stability of select mRNA populations—irrespective of their presence within the granule—through the sequestration of an mRNA decay factor; MARF1. While it has been suggested that P-bodies may play a role in regulating the decay of mRNAs through preferentially protecting their 5' end (12), to our knowledge these are the first data to establish a direct and causal role for P-bodies in regulating the decay of select mRNAs by modulating the activity of a decay factor.

### P-body regulation of MARF1 and mammalian oogenesis

MARF1 was first identified in the context of its role in promoting mammalian oogenesis, where MARF1<sup>-/-</sup> mouse oocytes arrest at the germinal vesicle (GV) stage of meiosis, fail to undergo cytoplasmic maturation, and experience meiotic arrest (19). During the growth of meiotically-competent GVs, transcriptional activity shuts down to nearly undetectable levels, requiring oocytes to tightly regulate existing mRNA populations in order to execute gene expression programs (36). Concomitant with this drop in transcription rates, P-bodies are lost during the early growth phase of the oocyte and RNP granules become reorganized in the cytoplasm (37). Similarly, P-body-like foci that form through the overexpression of human DCP1A in growing oocytes dynamically reduce in both number and size over the course of meiotic maturation (38). Interestingly, overexpressing the core P-body protein LSM14A in mouse GVs has been reported to impair GV maturation into fertilization-competent oocytes (39). This phenotype is strikingly similar to MARF1<sup>-/-</sup> oocytes, which also display defects in GV maturation (19). We demonstrate that disrupting endogenous P-bodies in human cells enhances the ability of MARF1 to repress targeted mRNAs. It is therefore plausible that P-bodies during the early stages of GV growth negatively regulate MARF1 activity. However, once sufficient GV growth has occurred, P-bodies dissociate thereby freeing MARF1 to interface with and degrade select transcripts at this critical stage of development.

In agreement with this model, MARF1 mutant oocytes which are predicted to be catalytically active but have a misfolded eGFP tag fused to the MARF1 C-terminus generates fertilization-incompetent oocytes that exhibit a wholly different phenotype to meiotically arrested MARF1<sup>-/-</sup> oocytes (40). These MARF1-eGFP oocytes displayed defects where meiotic completion was accelerated that was coincident with increased rates of aneuploidy. While the mechanism behind these observations was not described, we believe that generating a mis-folded eGFP tag at the C-terminal end of MARF1 likely interfered with the interaction site of EDC4, which we demonstrated is only 10 residues from the C-terminus. This is consistent with our model of P-body regulation of MARF1, where instead of generating a catalytically dead MARF1 mutant that leads to meiotic arrest in growing GVs, interfering with the C-terminus generates an overactive mutant of MARF1, which

is incapable of being antagonized by the P-bodies that are present in the early stages of oogenesis. Furthermore, as knocking down *Lsm14b* generates a highly similar phenotype to MARF1-eGFP oocytes (39), these observations point to a model where interfering with the ability of P-bodies to regulate MARF1 activity explains the generation of oocytes that attempt to accelerate through meiosis before sufficient growth has occurred. This, in turn, could lead to the dysregulated meiotic processes and chromosomal segregation defects that were described. However, although intriguing, this model remains to be tested in the context of mammalian oogenesis.

In summary, we have described a novel mode whereby P-bodies can directly regulate the stability of select mRNA populations by using the P-body protein EDC4 to sequester the MARF1 endoribonuclease and prevent it from degrading targeted transcripts. Whether this represents a unique mechanism or one that P-bodies use to regulate other RNA-binding proteins that effect mRNA decay remains to be seen.

### SUPPLEMENTARY DATA

Supplementary Data are available at NAR Online.

### ACKNOWLEDGEMENTS

This work was supported by a Canadian Institutes of Health Research (CIHR) grant (MOP-130425) and a Natural Sciences and Engineering Research Council of Canada (NSERC) Discovery grant (RGPIN-2022-04215) to M.R.F.; Fonds de Recherche du Québec- Santé (FRQS) Chercheur-Boursier Senior and CIHR New Investigator awards to M.R.F. W.R.B was supported by a NSERC Alexander Graham Bell CGS-D Fellowship.

### FUNDING

Canadian Institutes of Health Research (CIHR) [MOP-130425 to M.R.F.]; Natural Sciences and Engineering Research Council of Canada (NSERC) [RGPIN-2022-04215 to M.R.F.]; Fonds de Recherche du Québec- Santé (FRQS) (to M.R.F.); NSERC Alexander Graham Bell CGS-D Fellowship (to W.R.B.).

*Conflict of interest statement.* None declared.

### REFERENCES

1. Yamashita, A., Chang, T.-C., Yamashita, Y., Zhu, W., Zhong, Z., Chen, C.-Y.A. and Shyu, A.-B. (2005) Concerted action of poly(A) nucleases and decapping enzyme in mammalian mRNA turnover. *Nat. Struct. Mol. Biol.*, **12**, 1054–1063.
2. Chang, C.-T., Bercovich, N., Loh, B., Jonas, S. and Izaurralde, E. (2014) The activation of the decapping enzyme DCP2 by DCP1 occurs on the EDC4 scaffold and involves a conserved loop in DCP1. *Nucleic Acids Res.*, **42**, 5217–5233.
3. Braun, J.E., Truffault, V., Boland, A., Huntzinger, E., Chang, C.T., Haas, G., Weichenrieder, O., Coles, M. and Izaurralde, E. (2012) A direct interaction between DCP1 and XRN1 couples mRNA decapping to 5' exonucleolytic degradation. *Nat. Struct. Mol. Biol.*, **19**, 1324–1331.
4. Jonas, S. and Izaurralde, E. (2015) Towards a molecular understanding of microRNA-mediated gene silencing. *Nat. Rev. Genet.*, **16**, 421–433.

5. Coller, J. and Parker, R. (2004) Eukaryotic mRNA decapping. *Annu. Rev. Biochem.*, **73**, 861–890.
6. Tauber, D., Tauber, G. and Parker, R. (2020) Mechanisms and regulation of RNA condensation in RNP granule formation. *Trends Biochem. Sci.*, **45**, 764–778.
7. Brandmann, T., Fakim, H., Padamsi, Z., Youn, J.Y., Gingras, A.C., Fabian, M.R. and Jinek, M. (2018) Molecular architecture of LSM14 interactions involved in the assembly of mRNA silencing complexes. *EMBO J.*, **37**, e97869.
8. Nishimura, T., Padamsi, Z., Fakim, H., Milette, S., Dunham, W.H., Gingras, A.C. and Fabian, M.R. (2015) The eIF4E-Binding protein 4E-T is a component of the mRNA decay machinery that bridges the 5' and 3' termini of target mRNAs. *Cell Rep.*, **11**, 1425–1436.
9. Parker, R. and Sheth, U. (2007) P bodies and the control of mRNA translation and degradation. *Mol. Cell.*, **25**, 635–646.
10. Yu, J.H., Yang, W.H., Gulick, T., Bloch, K.D. and Bloch, D.B. (2005) Ge-1 is a central component of the mammalian cytoplasmic mRNA processing body. *RNA*, **11**, 1795–1802.
11. Sheth, U. and Parker, R. (2003) Decapping and decay of messenger RNA occur in cytoplasmic processing bodies. *Science*, **300**, 805–808.
12. Hubstenberger, A., Courel, M., Benard, M., Souquere, S., Ernoul-Lange, M., Chouaib, R., Yi, Z., Morlot, J.B., Munier, A., Fradet, M. *et al.* (2017) P-Body purification reveals the condensation of repressed mRNA regulons. *Mol. Cell.*, **68**, 144–157.
13. Fenger-Grøn, M., Fillman, C., Norrild, B. and Lykke-Andersen, J. (2005) Multiple processing body factors and the ARE binding protein TTP activate mRNA decapping. *Mol. Cell.*, **20**, 905–915.
14. Coller, J. and Parker, R. (2005) General translational repression by activators of mRNA decapping. *Cell*, **122**, 875–886.
15. Brothers, W.R., Hebert, S., Kleinman, C.L. and Fabian, M.R. (2020) A non-canonical role for the EDC4 decapping factor in regulating MARF1-mediated mRNA decay. *Elife*, **9**, e54995.
16. Bloch, D.B., Li, P., Bloch, E.G., Berenson, D.F., Galdos, R.L., Arora, P., Malhotra, R., Wu, C. and Yang, W. (2014) LMKB/MARF1 localizes to mRNA processing bodies, interacts with ge-1, and regulates IFI44L gene expression. *PLoS One*, **9**, e94784.
17. Youn, J.Y., Dunham, W.H., Hong, S.J., Knight, J.D.R., Bashkurov, M., Chen, G.I., Bagci, H., Rathod, B., MacLeod, G., Eng, S.W.M. *et al.* (2018) High-Density proximity mapping reveals the subcellular organization of mRNA-Associated granules and bodies. *Mol. Cell.*, **69**, 517–532.
18. Yao, Q., Cao, G., Li, M., Wu, B., Zhang, X., Zhang, T., Guo, J., Yin, H., Shi, L., Chen, J. *et al.* (2018) Ribonuclease activity of MARF1 controls oocyte RNA homeostasis and genome integrity in mice. *Proc. Natl. Acad. Sci.*, **115**, 11250–11255.
19. Su, Y.Q., Sugiura, K., Sun, F., Pendola, J.K., Cox, G.A., Handel, M.A., Schimenti, J.C. and Eppig, J.J. (2012) MARF1 regulates essential oogenic processes in mice. *Science*, **335**, 1496–1499.
20. Kanemitsu, Y., Fujitani, M., Fujita, Y., Zhang, S., Su, Y.Q., Kawahara, Y. and Yamashita, T. (2017) The RNA-binding protein MARF1 promotes cortical neurogenesis through its RNase activity domain. *Sci. Rep.*, **7**, 1155.
21. Nishimura, T., Fakim, H., Brandmann, T., Youn, J.-Y., Gingras, A.-C., Jinek, M. and Fabian, M.R. (2018) Human MARF1 is an endoribonuclease that interacts with the DCP1:2 decapping complex and degrades target mRNAs. *Nucleic Acids Res.*, **46**, 12008–12021.
22. Jinek, M., Eulalio, A., Lingel, A., Helms, S., Conti, E. and Izaurralde, E. (2008) The C-terminal region of ge-1 presents conserved structural features required for P-body localization. *RNA*, **14**, 1991–1998.
23. Luo, Y., Na, Z. and Slavoff, S.A. (2018) P-Bodies: composition, properties, and functions. *Biochemistry*, **57**, 2424–2431.
24. Jonas, S. and Izaurralde, E. (2013) The role of disordered protein regions in the assembly of decapping complexes and RNP granules. *Genes Dev.*, **27**, 2628–2641.
25. Di Stefano, B., Luo, E.-C., Haggerty, C., Aigner, S., Charlton, J., Brumbaugh, J., Ji, F., Rabano Jiménez, I., Clowers, K.J., Huebner, A.J. *et al.* (2019) The RNA helicase DDX6 controls cellular plasticity by modulating P-Body homeostasis. *Cell Stem Cell*, **25**, 622–638.
26. Yang, G., Smibert, C.A., Kaplan, D.R. and Miller, F.D. (2014) An eIF4E1/4E-T complex determines the genesis of neurons from precursors by translationally repressing a proneurogenic transcription program. *Neuron*, **84**, 723–739.
27. Na, Z., Luo, Y., Cui, D.S., Khitun, A., Smelyansky, S., Loria, J.P. and Slavoff, S.A. (2021) Phosphorylation of a human microprotein promotes dissociation of biomolecular condensates. *J. Am. Chem. Soc.*, **143**, 12675–12687.
28. Na, Z., Luo, Y., Schofield, J.A., Smelyansky, S., Khitun, A., Muthukumar, S., Valkov, E., Simon, M.D. and Slavoff, S.A. (2020) The NBDY microprotein regulates cellular RNA decapping. *Biochemistry*, **59**, 4131–4142.
29. D'Lima, N.G., Ma, J., Winkler, L., Chu, Q., Loh, K.H., Corpuz, E.O., Budnik, B.A., Lykke-Andersen, J., Saghatelian, A. and Slavoff, S.A. (2017) A human microprotein that interacts with the mRNA decapping complex. *Nat. Chem. Biol.*, **13**, 174–180.
30. Zhu, L., Kandasamy, S.K., Liao, S.E. and Fukunaga, R. (2018) LOTUS domain protein MARF1 binds CCR4-NOT deadenylase complex to post-transcriptionally regulate gene expression in oocytes. *Nat. Commun.*, **9**, 4031.
31. Su, Y.Q., Sun, F., Handel, M.A., Schimenti, J.C. and Eppig, J.J. (2012) Meiosis arrest female 1 (MARF1) has nuage-like function in mammalian oocytes. *Proc. Natl. Acad. Sci. U. S. A.*, **109**, 18653–18660.
32. Gillian-Daniel, D.L., Gray, N.K., Aström, J., Barkoff, A. and Wickens, M. (1998) Modifications of the 5' cap of mRNAs during xenopus oocyte maturation: independence from changes in poly(A) length and impact on translation. *Mol. Cell. Biol.*, **18**, 6152–6163.
33. Ma, J., Flemr, M., Strnad, H., Svoboda, P. and Schultz, R.M. (2013) Maternally recruited DCPIA and DCP2 contribute to messenger RNA degradation during oocyte maturation and genome activation in mouse1. *Biol. Reprod.*, **88**, 1–12.
34. Sankaranarayanan, M., Emenecker, R.J., Wilby, E.L., Jahnel, M., Trussina, I., Wayland, M., Alberti, S., Holehouse, A.S. and Weil, T.T. (2021) Adaptable p body physical states differentially regulate bicoid mRNA storage during early drosophila development. *Dev. Cell*, **56**, 2886–2901.
35. Buddika, K., Huang, Y.T., Ariyapala, I.S., Butrum-Griffith, A., Norrell, S.A., O'Connor, A.M., Patel, V.K., Rector, S.A., Slovan, M., Sokolowski, M. *et al.* (2021) Coordinated repression of pro-differentiation genes via P-bodies and transcription maintains drosophila intestinal stem cell identity. *Curr. Biol.*, **32**, 386–397.
36. Clarke, H.J. (2012) Post-transcriptional control of gene expression during mouse oogenesis. *Results Probl. Cell Differ.*, **55**, 1–21.
37. Flemr, M., Ma, J., Schultz, R.M. and Svoboda, P. (2010) P-body loss is concomitant with formation of a messenger RNA storage domain in mouse oocytes. *Biol. Reprod.*, **82**, 1008–1017.
38. Swetloff, A., Conne, B., Huarte, J., Pitetti, J.L., Nef, S. and Vassalli, J.D. (2009) Dcp1-bodies in mouse oocytes. *Mol. Biol. Cell*, **20**, 4951–4961.
39. Zhang, T., Li, Y., Li, H., Ma, X.S., Ouyang, Y.C., Hou, Y., Schatten, H. and Sun, Q.Y. (2017) RNA-associated protein LSM family member 14 controls oocyte meiotic maturation through regulating mRNA pools. *J. Reprod. Dev.*, **63**, 383–388.
40. Cao, G.Y., Li, M.Z., Wang, H., Shi, L.Y. and Su, Y.Q. (2018) Interference with the C-terminal structure of MARF1 causes defective oocyte meiotic division and female infertility in mice. *J. Biomed Res.*, **32**, 58–67.